

Anisotropic magnetism, resistivity, London penetration depth and magneto-optical imaging of superconducting $\text{K}_{0.80}\text{Fe}_{1.76}\text{Se}_2$ single crystals

R. Hu, K. Cho, H. Kim, H. Hodovanets, W. E. Straszheim, M. A. Tanatar, R. Prozorov, S. L. Bud'ko, P. C. Canfield
Ames Laboratory, U.S. DOE and Department of Physics and Astronomy, Iowa State University, Ames, IA 50011, USA
 (Dated: January 12, 2013)

Single crystals of $\text{K}_{0.80}\text{Fe}_{1.76}\text{Se}_2$ were successfully grown from a ternary solution. We show that although crystals form when cooling a near stoichiometric melt, crystals are actually growing out of a ternary solution that remains liquid to at least 850°C . We investigated their chemical composition, anisotropic magnetic susceptibility and resistivity, specific heat, thermoelectric power, London penetration depth and flux penetration via magneto-optical imaging. Whereas the samples appear to be homogeneously superconducting at low temperatures, there appears to be a broadened transition range close to $T_c \sim 30\text{ K}$ that may be associated with small variations in stoichiometry.

PACS numbers: 74.70.Xa, 74.25.Bt, 74.25F-, 74.25.Op

The iron-based superconductors have attracted intense research attention because of their high transition temperature and their possibly unconventional pairing mechanism, correlated to magnetism.^{1–4} Similar to cuprate superconductors, iron-based superconductors have layered structures; the planar Fe layers tetrahedrally coordinated by As or chalcogen anions (Se or Te) are believed to be responsible for superconductivity. Stacking of the FeAs building blocks with alkali, alkaline earth or rare earth oxygen spacer layers forms the basic classes of iron arsenic superconductors in these compounds: 111-type AFeAs ⁵, 122-type AFe_2As_2 ^{6–9}, 1111-type ROFeAs ^{10,11} and more complex block containing phases, e.g. $\text{Sr}_2\text{VO}_3\text{FeAs}$ ¹², $\text{Sr}_3\text{Sc}_2\text{Fe}_2\text{As}_2\text{O}_5$ ¹³, $\text{Sr}_4\text{Sc}_2\text{Fe}_2\text{As}_2\text{O}_6$.¹⁴ The simple binary 11-type iron chalcogenide has no spacer layers and superconductivity can be induced by doping FeTe with S¹⁵ or Se.¹⁶ Different from the other iron-based superconductors, FeSe is a superconductor¹⁷, $T_c \sim 8\text{ K}$, with no static magnetic order and its transition temperature can be increased up to 37 K by applying pressure¹⁸ or 15 K in $\text{FeSe}_{0.5}\text{Te}_{0.5}$.¹⁶ More recently, superconductivity above 30 K has been reported in $\text{A}_x\text{Fe}_{2-y}\text{Se}_2$ ($\text{A} = \text{K}, \text{Cs}, \text{Rb}$ or Tl)^{19–22}, a compound with the same unit cell structure as the AFe_2As_2 compounds. These new compounds generally have a width of formation, show strong dependence of electrical transport properties on its stoichiometry/Fe vacancy and are in very close proximity to an insulating state.^{22,23} The growth of single crystals of $\text{K}_x\text{Fe}_{2-y}\text{Se}_2$ has been reported in a number of publications using various claimed growth methods: self-flux growth²⁰, Bridgman method.²³ Due to the off-stoichiometric nature of the $\text{K}_x\text{Fe}_{2-y}\text{Se}_2$, wide ranges of the values of x, y ($0.6 \leq x < 1$ and $0 \leq y \leq 0.59$)^{20–29} have been reported for the superconducting crystals with similar T_c values ($\sim 31–33\text{ K}$) from several groups. This raises the question what the correlation between superconductivity and stoichiometry is, if there is any, and whether there is a uniformity problem with the single crystal samples. Thus well controlled samples are needed and it is desirable to check the homogeneity of the superconducting crystals and understand their growth.

In this work, we will try to clarify the growth details and present elemental analysis, anisotropic magnetization and resistivity data, as well as measurements of heat capacity, thermoelectrical power, London penetration depth and flux penetration on $\text{K}_{0.80}\text{Fe}_{1.76}\text{Se}_2$ single crystals.

Single crystals of $\text{K}_x\text{Fe}_{2-y}\text{Se}_2$ were first grown from $\text{K}_{0.8}\text{Fe}_2\text{Se}_2$ melt, as described in Ref. 20. First the FeSe precursor was prepared by reacting stoichiometric Fe and Se at 1050°C . Then K and FeSe with a nominal composition of $\text{K}_{0.8}\text{Fe}_2\text{Se}_2$ were placed in an alumina crucible that was sealed in an amorphous silica tube. Due to potassium attack on the silica tube, this primary ampoule was sealed into a secondary, larger silica tube to prevent exposure to air if the first ampoule degraded enough to crack. The growth was placed in a furnace in a vented enclosure and heated to 1050°C , where it was held for a 2 hours soak. The furnace temperature was then and slowly lowered to 750°C over 50 hours; the furnace was then turned off and the sample "furnace cooled" over an additional 10 hours. Once the ampoules were opened, large ($\sim 1 \times 1 \times 0.02\text{ cm}^3$) dark shiny crystals could be mechanically separated from the solidified melt. The crystals are moderately air-sensitive and should be handled under an Ar atmosphere.

The above growth procedure clearly is not simply the cooling of a stoichiometric melt to form a congruently melting, line compound. There is clear loss of K from the melt (as seen by the attack of the inner ampoule) and there is a clear mixed phase resultant sample, consisting of the desired single crystalline phase separated by fine polycrystalline material. In order to better establish the nature of the growth of $\text{K}_x\text{Fe}_{2-y}\text{Se}_2$ the above procedure was repeated for a starting composition of KFe_3Se_3 . The sample was heated to 1050°C , held for 2 hours and slowly cooled to 850°C at which point the remaining solution was decanted. The resulting crystals were about $1/2$ the area and thickness of the the samples cooled to 750°C , but they were well formed and no longer embedded in solidified flux. This result clearly shows that $\text{K}_x\text{Fe}_{2-y}\text{Se}_2$ crystals are grown out of a ternary melt.

Crystals were characterized by powder x-ray diffrac-

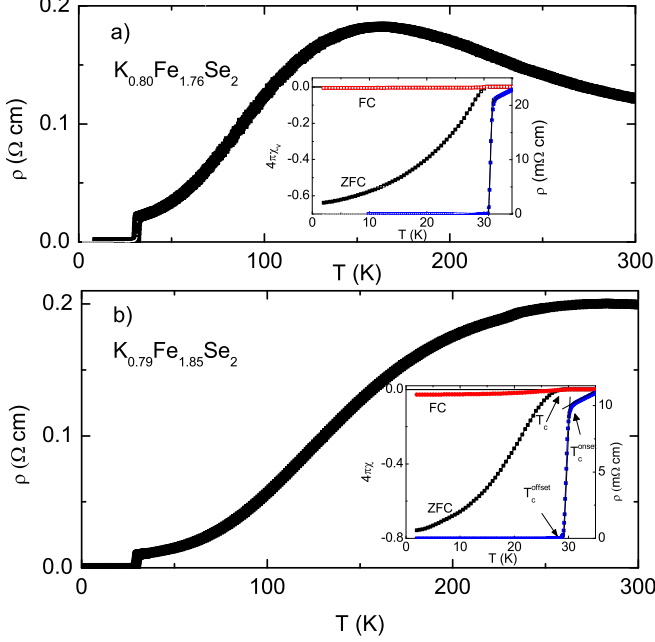


FIG. 1: Comparison of the in-plane resistivity, and low temperature magnetic susceptibility of two types of $K_xFe_{2-y}Se_2$ single crystals, a) furnace cooled; b) decanted sample. Inset shows the low temperature region of the resistivity (to the right axis) together with zero-field-cooled and field-cooled magnetic susceptibility in a field of 50 Oe.

tion using a Rigaku Miniflex X-ray diffractometer. The actual chemical composition was determined by wavelength dispersive x-ray spectroscopy (WDS) in a JEOL JXA-8200 electron microscope. Magnetic susceptibility was measured in a Quantum Design MPMS, SQUID magnetometer. In plane AC resistivity ρ_{ab} was measured by a standard four-probe configuration. Measurement of ρ_c was made in the two-probe configuration. Contacts were made by using a silver alloy. For ρ_c , contacts were covering the whole ab plane area.³⁰ Thermoelectrical power measurements were carried out by a dc, alternating temperature gradient (two heaters and two thermometers) technique.³¹ Heat capacity data were collected using a Quantum Design PPMS. The in-plane London penetration depth was measured by using a tunnel-diode resonator (TDR) oscillating at 14 MHz and at temperature down to 0.5 K.³² Magneto-optical imaging was conducted by utilizing the Faraday effect in bismuth-doped iron garnet indicators with in-plane magnetization.³³ A flow-type liquid 4He cryostat with sample in vacuum was used. The sample was positioned on top of a copper cold finger and an indicator was placed on top of the sample. The cryostat was positioned under polarized-light reflection microscope and the color images could be recorded on video and high-resolution CCD cameras. When linearly polarized light passes through the indicator and reflects off the mirror sputtered on its bottom, it picks up a dou-

ble Faraday rotation proportional to the magnetic field intensity at a given location on the sample surface. Observed through the (almost) crossed analyzer, we recover a 2D image.³⁴

The x-ray diffraction pattern can be indexed using space group I4/mmm. The lattice parameters refined by Rietica were $a = 3.8897(8)\text{\AA}$ and $c = 14.141(3)\text{\AA}$. They are in good agreement with the previous reported values in Ref. 20 ($a = 3.8912\text{\AA}$, $c = 14.139\text{\AA}$), but disagree with Ref. 19 ($a = 3.9136(1)\text{\AA}$, $c = 14.0367(7)\text{\AA}$) and Ref. 27 ($a = 3.9034\text{\AA}$, $c = 14.165\text{\AA}$), in lattice constant c . It is probably due to the different stoichiometry of the crystals.

Previous reported stoichiometries of $K_xFe_{2-y}Se_2$ crystals were determined by the semi-quantitative Energy Dispersive X-ray (EDX) spectroscopy.^{20–29} Here we performed precise measurement of the stoichiometry using WDS. Twelve measurement spots were spread uniformly across the crystal surfaces of dimension approximately $3 \times 3\text{ mm}^2$. All of the spots showed consistent results. By averaging 12 spots, the stoichiometry was determined to be $K : Fe : Se = 0.80(2) : 1.76(2) : 2.00(3)$ for the crystal grown from solidified melt and $K : Fe : Se = 0.79(2) : 1.85(4) : 2.00(4)$ for the crystal grown from solution, where the atomic numbers of K and Fe are normalized to two Se per formula unit and the standard deviation σ is taken as the compositional error and shown in parentheses after value. The spread of composition, the difference between the maximum and minimum values of the measurements, is 0.07, 0.06 and 0.10 for K, Fe and Se respectively for crystal grown from solidified melt and 0.04, 0.12 and 0.09 for crystal grown from solution, roughly within 3σ of a normal distribution of random variable. The crystals grown from solution have very similar composition to the furnace cooled samples, with only a little higher concentration of Fe.

Basic, temperature dependent electrical resistivity and magnetization measurements were performed on crystals grown by both the furnace cooled and decanted methods. The in-plane resistivity of the furnace cooled sample is very similar to that of earlier reports.^{20,23} There is a broad resistive maxima centered near 160 K followed by a lower temperature drop by nearly a factor of 6 ($\rho(300K)/\rho(35K)$). There is a sharp transition to a zero resistance state. The inset to Fig. 1a shows the low temperature resistivity as well as the in-plane, magnetic susceptibility ($H=50$ Oe). The superconducting transition temperature, $T_c = 30.1\text{ K}$, can be inferred by the first deviation of the zero-field-cooled curve from normal magnetic susceptibility. It is consistent with the $T_c^{offset} = 30.9\text{ K}$, inferred from resistivity. The transition is sharp with a width of 0.7 K and $T_c^{onset} = 31.6\text{ K}$.

The in-plane resistivity of single crystals grown out of solution (the decanted samples) is shown in Fig. 1b. It exhibits a broad maximum around 280 K and becomes superconducting below 30 K. The inset shows the in-plane magnetic susceptibility ($H = 50\text{ Oe}$) and resistivity

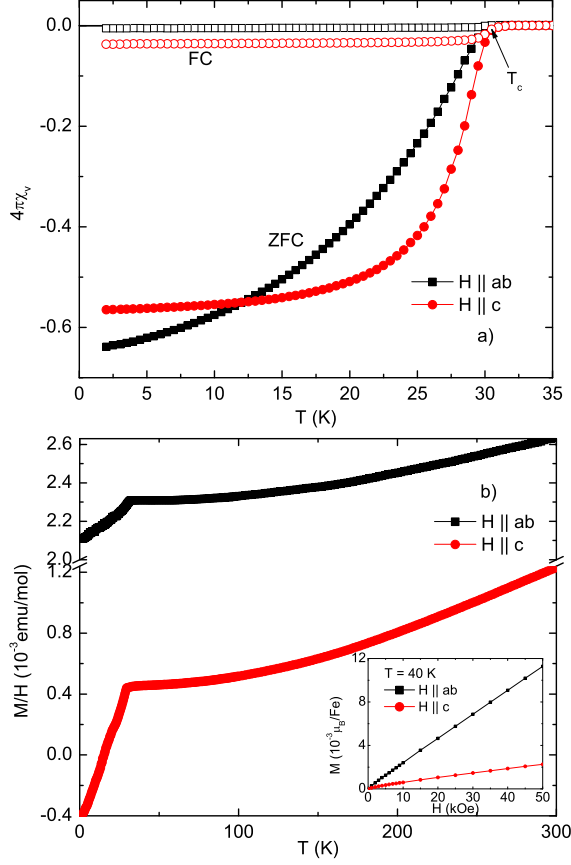


FIG. 2: a) Temperature dependence of low field ($H = 50$ Oe) magnetic susceptibility for $H||ab$ and $H||c$; b) Magnetic susceptibility M/H and T_c measured in 50 kOe for two field directions. Inset shows field dependence of magnetization at 40 K for both field directions.

at low temperature. Superconducting transition temperature, $T_c = 29.0$ K, can be inferred by the first deviation of the zero-field-cooled curve from normal magnetic susceptibility. It is consistent with the $T_c^{offset} = 29$ K, inferred from resistivity. The transition is sharp with a width of 1 K and $T_c^{onset} = 30.0$ K. The temperature of the broad resistive peak in Fig. 1b is higher than the one shown in Fig. 1a and the T_c value is slightly lower. Wang *et al.* showed that the position of the hump is sensitive to Fe deficiency.²³ With decreasing Fe deficiency, the hump shifts to higher temperature. This may imply that our decanted crystal has a slightly higher Fe concentration, reasonable for a crystal grown out of solution with a greater excess of Fe-Se. Even with these slight differences, the WDS analysis and the data shown in figure 1 demonstrate that these are closely related compositions with very similar properties. Given the somewhat larger size of the furnace cooled samples, as well as their similarity to samples from earlier reports, for the rest of this paper we will focus their fuller characterization.

Figure 2a shows the magnetic susceptibility of

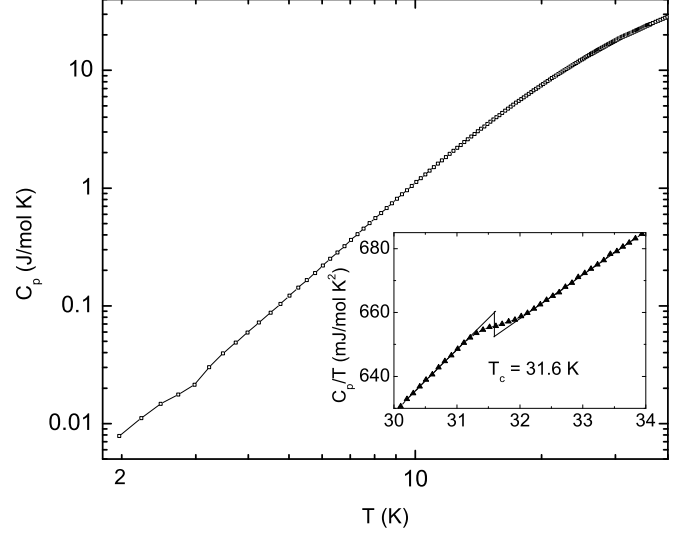


FIG. 3: Heat capacity as a function of temperature on a log-log plot. Inset shows the heat capacity jump at the superconducting transition. The solid line is an isoentropic estimate of T_c and ΔC_p .

$\text{K}_{0.80}\text{Fe}_{1.76}\text{Se}_2$ for two directions of an applied field of 50 Oe. For magnetic field along c axis, a correction of demagnetization for a thin rectangular sample has been made. For $H || ab$, the zero-field-cooled (ZFC) curve decreases slowly with temperature and for $H || c$ the transition becomes sharper. Similar behavior can be seen in $\text{Tl}_{0.58}\text{Rb}_{0.42}\text{Fe}_{1.72}\text{Se}_2$.³⁵ This temperature dependence of the ZFC curve is similar to an inhomogeneous superconductor with a range of transition temperatures and may be related to the small spread of stoichiometry found in WDS data. Both of the zero-field-cooled (ZFC) curves in Fig. 2a approach -0.6 consistent with bulk superconductivity and T_c inferred from both curves is the same, $T_c = 30.1 \pm 0.1$ K, within experimental error.

The magnetic susceptibility M/H ($H = 50$ kOe) as a function of temperature for both field directions is shown in Fig. 2b. Similar temperature dependence is observed for both field directions, i.e. M/H decreases almost linearly with decreasing temperature above 150 K and shows a sudden drop below 30 K associated with superconductivity. χ_{ab} is clearly larger than χ_c over the whole temperature range. The inset to Fig. 2b shows the magnetization as a function of magnetic field at $T = 40$ K. Magnetization is linear with magnetic field for both directions. It also should be noted that the magnitude of magnetization, even at highest field, is very small, $10^{-3} \mu_B/\text{Fe}$. This indicates that there are no ferromagnetic impurities or Curie-Weiss like, local Fe moments and the system might be deep in an antiferromagnetic state, similar to what was suggested for $\text{Cs}_{0.8}\text{Fe}_2\text{Se}_{1.96}$ ³⁶ and $\text{K}_{0.8}\text{Fe}_{1.6}\text{Se}_2$ ³⁷, or in a non-magnetic state.

Heat capacity data was collected to verify the bulk

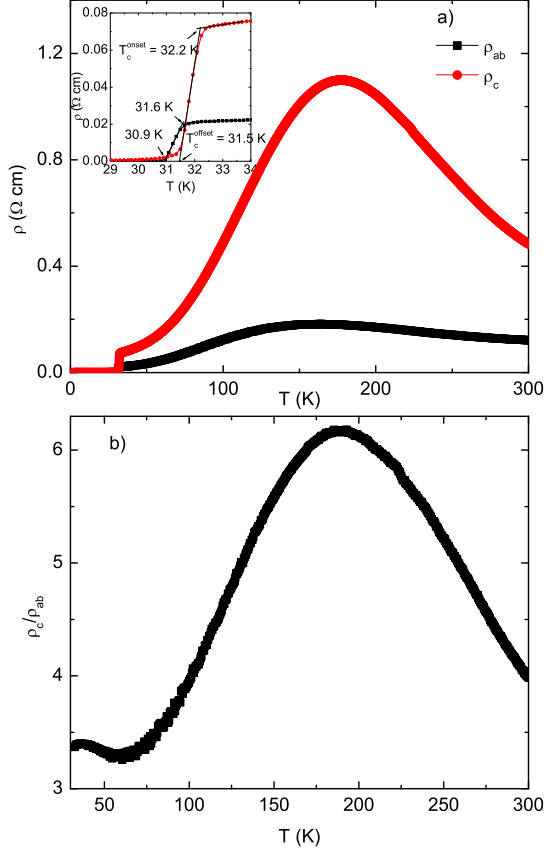


FIG. 4: a) Anisotropic resistivity as a function of temperature. Inset is an expanded view around the transition. b) Anisotropy of resistivity vs temperature.

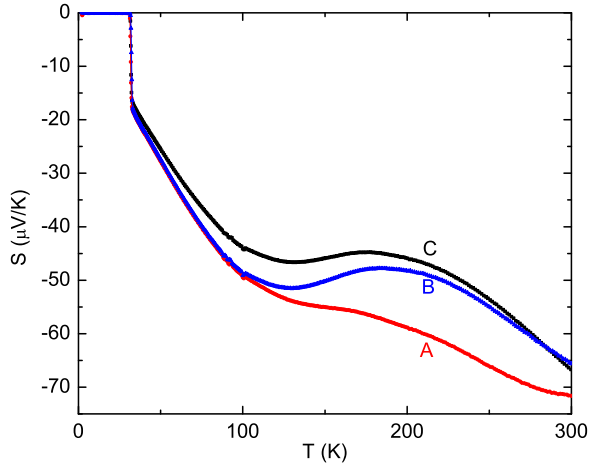


FIG. 5: Thermoelectric power as a function of temperature. Samples A and B use silver paste as contact (contact resistance $\sim 1 - 3 \text{ k}\Omega$). Sample C uses silver wires attached by In-Sn solder as contact (contact resistance $\sim 200 \text{ }\Omega$).

thermodynamic nature of the superconducting transition. C_p vs T at low temperature is shown in Fig. 3 on a log-log plot. In the superconducting state, below 15 K, C_p roughly follows a T^3 power law. This implies a dominant phonon contribution and a very small electronic term. C_p/T vs T is plotted in the inset for $T \sim T_c$ and a clear jump of heat capacity associated with the superconducting transition at 31.6 K is seen and $\Delta C_p/T = 7.7 \text{ mJ/mol K}^2$, can be identified. If we assume the value of normal state electronic heat capacity coefficient $\gamma_n = 5.8 \text{ mJ/mol K}^2$ (as in Ref. 38), $\Delta C_p/\gamma_n T = 1.33$ of $\text{K}_{0.80}\text{Fe}_{1.76}\text{Se}_2$ is close to the weak coupling BCS value and is in variance with the strong coupling conclusion in Ref. 38. On the other hand, this more likely implies that a reliable conclusion about the coupling strength can not be made due to the difficulty of estimating the normal state electronic contribution γ_n .

Anisotropic resistivity as a function of temperature is shown in Fig. 4a. It is clear that there is a broad maximum peak around 160 K for ρ_{ab} and 180 K for ρ_c . The difference of maximum positions suggest that they result from a crossover rather than transition. The temperature range of this broad maxima does not correlate with any anomalies in magnetic susceptibility. The anisotropy is probably due to the layered structure of $\text{K}_{0.80}\text{Fe}_{1.76}\text{Se}_2$. Figure 4b shows the anisotropy ρ_c/ρ_{ab} , reaches the maximum of 6 around 180 K and decreases to 4 around 300 K. It is comparable to the anisotropy of AFe_2As_2 .³⁹ But a much larger resistivity anisotropy of 30-45 was reported in $(\text{Ti,K})\text{Fe}_x\text{Se}_2$ ³⁵, this implies that the specific composition influences carrier tunneling significantly. An expanded view around the superconducting transition is shown in the inset to Fig. 4a. For both of the current directions, the transition width is about 0.7 K, but T_c for ρ_c is slightly higher than that of ρ_{ab} . The transition temperatures for the two current directions are very close to the one inferred from the heat capacity measurement using an isoentropic construction, as well as resistivity and susceptibility measurements.

The thermoelectrical power (TEP) as a function of temperature is shown in Fig. 5. We present results for three different samples: for samples A and B silver paste was used for electrical and thermal contact, for sample C silver wires were soldered to the sample by In-Sn solder and then electrical / thermal contact was established between the wires and the contact pads by silver paste. For all three samples T_c inferred from $S(T) = 0$ is 31.6 K, consistent with all of our previous measurements. The data for three samples are similar in the whole temperature range. The origin of local minimum and maximum in 100 – 200 K is not clear, but is very likely to be associated with the multiband structure of $\text{K}_{0.80}\text{Fe}_{1.76}\text{Se}_2$ and the crossover (metal-like at low temperature observed in resistivity. Negative sign of thermopower indicates that electron like carriers are dominant, thus in agreement with the observation of electron only pockets at the Fermi surface by ARPES.²⁶ The large absolute value of S above 50 K is noteworthy and is consistent with high normal

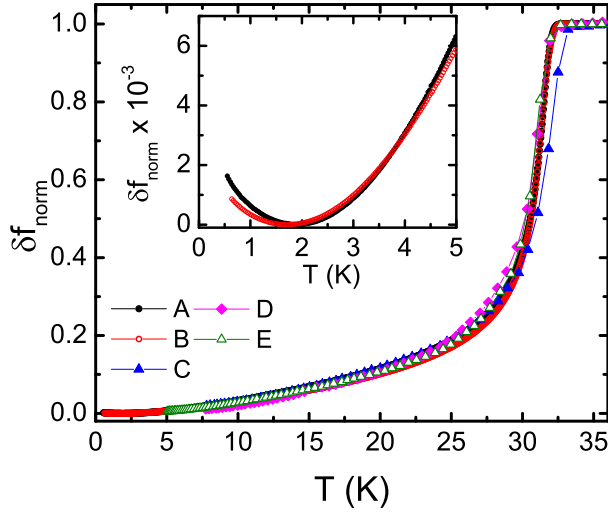


FIG. 6: Normalized London penetration depth expressed via resonant frequency shift, $\Delta f_{norm} = (f(T) - f(T_c))/(f(T_c) - f(T_{min}))$ proportional to magnetic susceptibility. $f(T_{min})$ is the resonant frequency at the lowest temperature $\simeq 0.5$ K. $f(T_c)$ is the frequency in the normal state right above T_c . Inset shows an upturn, presumably due to paramagnetic ions and/or impurities below 2 K from two samples A and B.

state resistivity.

London penetration depth measurements with good reproducibility were performed on several single crystal samples. In order to compare between the samples, we plot in Fig. 6 normalized frequency shift, proportional to differential magnetic susceptibility, $\delta f_{norm} = (f(T) - f(T_c))/(f(T_c) - f(T_{min}))$, where $f(T_{min})$ is the resonant frequency at the lowest temperature $\simeq 0.5$ K and $f(T_c)$ is the frequency in the normal state right above T_c . The samples show consistent behavior indicating little or no variation within the batch. The transition itself is quite unusual - it shows quite a sharp onset, but then is smeared almost over the entire temperature interval. In this work, it might be due to off-stoichiometry of iron and/or impurities. In principle, it is also possible that the observed behavior is indicative of strongly anisotropic gap function or even nodes, but we cannot rule out simple variation of the superconducting properties as a cause of such unusual superconducting transition in $K_{0.80}Fe_{1.76}Se_2$. In addition, there is a clear upturn at low temperatures. It has been shown on both, high- T_c cuprates⁴⁰ and 1111 pnictides⁴¹ that this upturn is caused by the paramagnetic ions.

To gain further insight into the homogeneity of the superconducting state and, roughly, estimate critical current density, we performed magneto-optical imaging. A magneto-optical image of a trapped flux is shown in Fig. 7. In the experiment the sample was cooled in a 2 kOe magnetic field from 40 K to 5 K. We did not observe any noticeable Meissner expulsion, similar to other 122 pnictides.⁴² When magnetic field was turned off, it revealed a typical “Bean” roof, again similar to other pnictide superconductors.^{43,44} As can be seen in Fig. 7, mag-

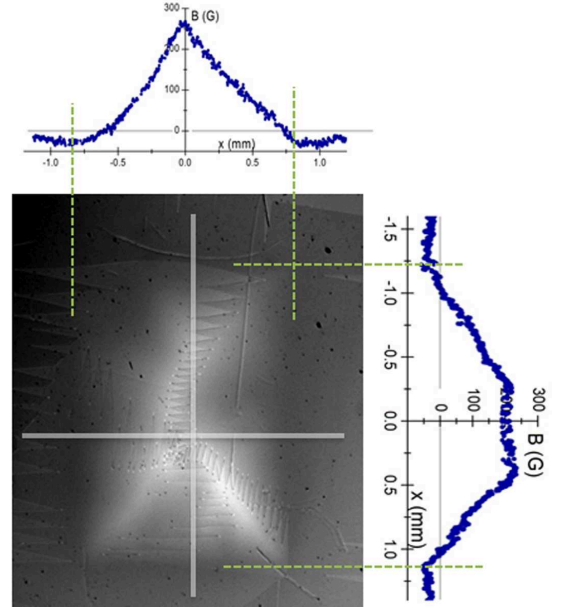


FIG. 7: Magneto-optical image of single crystal $K_{0.80}Fe_{1.76}Se_2$

netic flux distribution is quite uniform and is definitely consistent with the bulk superconducting nature of the material. However, some macroscopic variations (upper left corner) might indicate some smooth variation of stoichiometry across the sample and may help to explain the broadened transition curves. In order to quantify the critical state, Fig. 7 also shows profiles of the magnetic induction taken along two lines (shown in the figure). The remanence reaches about 250 Oe. A simple one-dimensional estimate, using

$$\frac{4\pi}{c} j_c = \frac{dB}{dx}$$

gives:

$$j_c = \frac{250}{0.77} \frac{10}{4\pi} \approx 2.6 \times 10^3 \text{ A/cm}^2$$

Of course, this estimate is very crude, but shows that the current samples cannot support large critical current density even at low temperatures. Similar numbers are estimated from the magnetization measurements. Nevertheless, magneto-optical imaging is consistent with bulk superconducting nature of $K_{0.80}Fe_{1.76}Se_2$ and shows that it is not filamentary or phase separated, but rather shows smooth variation of the stoichiometry.

In summary, single crystals of $K_xFe_{2-y}Se_2$ have been grown via two related methods. In both cases $T_c \sim 30$ K, with the furnace cooled crystals having $K_{0.80}Fe_{1.76}Se_2$ composition and $T_c = 30$ K (from magnetization) and decanted crystals having composition $K_{0.83}Fe_{1.86}Se_{2.09}$ and $T_c = 29$ K (from magnetization). We found moderate anisotropy in both magnetic susceptibility and electrical resistivity with $\chi_{ab}/\chi_c \sim 2$ and $\rho_c/\rho_{ab} \sim 4$ at 300

K. Broadened transitions seen in several measurements imply a small variation of stoichiometry of the crystal, consistent with what was shown by WDS analysis. It has also been shown that the critical current density of the $K_{0.80}Fe_{1.76}Se_2$ is only on the order of $10^3 A/cm^2$, much smaller than those of FeAs superconductors.⁴⁵

Note added. During the preparation of this paper, a preprint was posted on arxiv.org showing similar studies of anisotropy in electrical transport and magnetization of $K_xFe_{2-y}Se_2$.⁴⁶ The results of are consistent with ours.

I. ACKNOWLEDGEMENTS

This work was carried out at the Iowa State University and supported by the AFOSR-MURI grant #FA9550-09-

1-0603 (R. Hu and P. C. Canfield). Part of this work was performed at Ames Laboratory, US DOE, under contract # DE-AC02-07CH 11358 (K. Cho, H. Kim, H. Hodovanets, W. E. Straszheim, M. A. Tanatar, R. Prozorov, S. L. Bud'ko and P. C. Canfield). S. L. Bud'ko also acknowledges partial support from the State of Iowa through Iowa State University. R. Prozorov acknowledges support from the Alfred P. Sloan Foundation.

-
- ¹ Kenji Ishida, Yusuke Nakai, and Hideo Hosono, J. Phys. Soc. Jpn., **78** 062001 (2009).
 - ² M. D. Lumsden and A. D. Christianson, J. Phys.: Condens. Matter, **22** 203203 (2010).
 - ³ Paul C. Canfield and Sergey L. Bud'ko, Annual Review of Condensed Matter Physics, **1**, 27 (2010).
 - ⁴ Johnpierre Paglione and Richard L. Greene, Nature Physics **6**, 645 (2010).
 - ⁵ X. C. Wang, Q. Q. Liu, Y. X. Lv, W. B. Gao, L. X. Yang, R. C. Yu, F. Y. Li, C. Q. Jin, Solid State Commun. **148**, 538 (2008).
 - ⁶ M. Rotter, M. Tegel, and D. Johrendt, Phys. Rev. Lett. **101**, 107006 (2008).
 - ⁷ Athena S. Sefat, Rongying Jin, Michael A. McGuire, Brian C. Sales, David J. Singh, and David Mandrus, Phys. Rev. Lett. **101**, 117004 (2008).
 - ⁸ N. Ni, M. E. Tillman, J.-Q. Yan, A. Kracher, S. T. Hannahs, S. L. Bud'ko, and P. C. Canfield, Phys. Rev. B **78**, 214515 (2008).
 - ⁹ A. Leithe-Jasper, W. Schnelle, C. Geibel, and H. Rosner, Phys. Rev. Lett. **101**, 207004 (2008).
 - ¹⁰ Y. Kamihara, T. Watanabe, M. Hirano, and H. Hosono, J. Am. Chem. Soc. **130**, 3296 (2008).
 - ¹¹ X. H. Chen, T. Wu, G. Wu, R. H. Liu, H. Chen, and D. F. Fang, Nature **453**, 761 (2008).
 - ¹² X. Zhu, F. Han, G. Mu, P. Cheng, B. Shen, B. Zeng, and H. H. Wen, Phys. Rev. B **79**, 220512 (2009).
 - ¹³ X. Zhu, F. Han, G. Mu, B. Zeng, P. Cheng, B. Shen, H. H. Wen, Phys. Rev. B **79** 024516 (2009).
 - ¹⁴ G. F. Chen, T. L. Xia, H. X. Yang, J. Q. Li, P. Zheng, J. L. Luo, N. L. Wang, Supercond. Sci. Tech. **22**, 072001 (2009).
 - ¹⁵ Rongwei Hu, Emil S. Bozin, J. B. Warren, and C. Petrovic, Phys. Rev. B **80**, 214514 (2009).
 - ¹⁶ Y. Mizuguchi, Y. Hara, K. Deguchi, S. Tsuda, T. Yamaguchi, K. Takeda, H. Kotegawa, H. Touand, Y. Takano, Supercond. Sci. Tech., **23** 054013 (2010).
 - ¹⁷ F. C. Hsu, J. Y. Luo, K. W. The, T. K. Chen, T. W. Huang, P. M. Wu, Y. C. Lee, Y. L. Huang, Y. Y. Chu, D. C. Yan and M. K. Wu, Proc. Nat. Acad. Sci. **105**, 14262 (2008).
 - ¹⁸ S. Medvedev, T. M. McQueen, I. Trojan, T. Palasyuk, M. I. Eremets, R. J. Cava, S. Naghavi, F. Casper, V. Ksenofontov, G. Wortmann and C. Felser, Nature Mater., **8** 630 (2009).
 - ¹⁹ Jiangang Guo, Shifeng Jin, Gang Wang, Shunchong Wang, Kaixing Zhu, Tingting Zhou, Meng He and Xiaolong Chen, Phys. Rev. B **82**, 180520 (2010).
 - ²⁰ J. J. Ying, X. F. Wang, X. G. Luo, A. F. Wang, M. Zhang, Y. J. Yan, Z. J. Xiang, R. H. Liu, P. Cheng, G. J. Ye, X. H. Chen, arXiv:1012.5552v1 (2010).
 - ²¹ Chun-Hong Li, Bing Shen, Fei Han, Xiyu Zhu, Hai-Hu Wen, arXiv:1012.5637v2 (2010).
 - ²² Minghu Fang, Hangdong Wang, Chiheng Dong, Zujuan Li, Chunmu Feng, Jian Chen, H. Q. Yuan, arXiv:1012.5236 (2010).
 - ²³ D. M. Wang, J. B. He, T.-L. Xia, G. F. Chen, arXiv:1101.0789v1 (2011).
 - ²⁴ Y. Zhang, L. X. Yang, M. Xu, Z. R. Ye, F. Chen, C. He, J. Jiang, B. P. Xie, J. J. Ying, X. F. Wang, X. H. Chen, J. P. Hu, D. L. Feng, arXiv:1012.5980v1 (2010).
 - ²⁵ I.R. Shein, A.L. Ivanovskii, arXiv:1012.5164 (2010).
 - ²⁶ T. Qian, X.-P. Wang, W.-C. Jin, P. Zhang, P. Richard, G. Xu, X. Dai, Z. Fang, J.-G. Guo, X.-L. Chen, H. Ding, arXiv:1012.6017 (2010).
 - ²⁷ Yoshikazu Mizuguchi, Hiroyuki Takeya, Yasuna Kawasaki, Toshinori Ozaki, Shunsuke Tsuda, Takahide Yamaguchi and Yoshihiko Takano, Appl. Phys. Lett. **98**, 042511 (2011).
 - ²⁸ D. A. Torchetti, M. Fu, D. C. Christensen, K. J. Nelson, T. Imai, H. C. Lei, C. Petrovic, arXiv:1101.4967v1 (2011).
 - ²⁹ P. Zavalij, W. Bao, X. F. Wang, J. J. Ying, X. H. Chen, D. M. Wang, J. B. He, X. Q. Wang, G.F. Chen, P-Y Hsieh, Q. Huang, M. A. Green, arXiv:1101.4882 (2011).
 - ³⁰ Jeffrey E. Marchese, Matteo Cirillo, and Niels Grøbech-Jensen, Phys. Rev. B **79**, 094517 (2009).
 - ³¹ Eundeok Mun, Sergey L. Bud'ko, Milton S. Torikachvili, and Paul C. Canfield, Meas. Sci. Technol. **21**, 21055104(2010).
 - ³² R. Prozorov and R.W. Giannetta, Supercond. Sci. Tech. **19**, R41 (2006).
 - ³³ L. A. Dorosinskii, M. V. Indenbom, V. I. Nikitenko, Yu. A. Ossip'yan, A. A. Polyanskii, and V. K. Vlasko-Vlasov, Physica C **203**, 149 (1992).

- ³⁴ Ch. Jooss, J. Albrecht, H. Kuhn, S. Leonhardt, and H. Kronmuller, Rep. Prog. Phys. 65, 651 (2002).
- ³⁵ Hangdong Wang, Chihen Dong, Zujuan Li, Shasha Zhu, Qianhui Mao, Chunmu Feng, H. Q. Yuan, Minghu Fang, arXiv:1101.0462v1 (2011).
- ³⁶ Z. Shermadini, A. Krzton-Maziopa, M. Bendele, R. Khasanov, H. Luetkens, K. Conder, E. Pomjakushina, S. Weyeneth, V. Pomjakushin, O. Bossen, A. Amato, arXiv:1101.1873v1 (2011).
- ³⁷ Wei Bao, Q. Huang, G. F. Chen, M. A. Green, D. M. Wang, J. B. He, X. Q. Wang, Y. Qiu, arXiv:1102.0830 (2011).
- ³⁸ Bin Zeng, Bing Shen, Genfu Chen, Jianbao He, Duming Wang, Chunhong Li, Hai-Hu Wen, arXiv:1101.5117 (2011).
- ³⁹ M. A. Tanatar, N. Ni, G. D. Samolyuk, S. L. Bud'ko, P. C. Canfield, R. Prozorov, Phys. Rev. B 79, 134528 (2009).
- ⁴⁰ R. Prozorov and R.W. Giannetta, P. Fournier and R.L. Greene, Phys. Rev. Lett. 85, 3700 (2000).
- ⁴¹ C. Martin, M. E. Tillman, H. Kim, M. A. Tanatar, S. K. Kim, A. Kreyssig, R. T. Gordon, M. D. Vannette, S. Nandi, V. G. Kogan, S. L. Bud'ko, P. C. Canfield, A. I. Goldman, and R. Prozorov
- ⁴² R. Prozorov, M. A. Tanatar, Bing Shen, Peng Cheng, Hai-Hu Wen, S. L. Bud'ko, and P. C. Canfield, Phys. Rev. B 82, 180513(R) (2010).
- ⁴³ R. Prozorov, M. E. Tillman, E. D. Mun, P. C. Canfield, New Journal of Physics 11, 035004 (2009).
- ⁴⁴ R. Prozorov, N. Ni, M. A. Tanatar, V. G. Kogan, R. T. Gordon, C. Martin, E. C. Blomberg, P. Prommapan, J. Q. Yan, S. L. Bud'ko, and P. C. Canfield, Phys. Rev. B 78, 224506 (2008).
- ⁴⁵ M A Tanatar, N Ni, S L Bud'ko, P C Canfield and R Prozorov, Supercond. Sci. Technol., 23 054002 (2010).
- ⁴⁶ Hechang Lei, C. Petrovic, arXiv:1102.1010 (2011).